Available online at www.sciencedirect.com
ScienceDirect
Journal of Bionic Engineering 9 (2012) 224–233

Preparation of Mesoporous Nano-Hydroxyapatite Using a Surfactant Template Method for Protein Delivery

Xiaodong Wu[1,2], Xiaofeng Song[2], Dongsong Li[1], Jianguo Liu[1], Peibiao Zhang[2], Xuesi Chen[2]

1. *Department of Bone and Joint Surgery*, *First Hospital of Jilin University*, *Changchun* 130021, *P. R. China*
2. *Key Laboratory of Polymer Ecobiomaterials*, *Changchun Institute of Applied Chemistry*, *Chinese Academy of Sciences*, *Changchun* 130022, *P. R. China*

Abstract

Mesoporous nano-hydroxyapatite (n-HA) has gained more and more attention as drug storage and release hosts. The aim of this study is to observe the effect of the ratio of surfactant to the theoretical yield of HA on the mesoporous n-HA, then to reveal the effect of the mesoporous nanostructure on protein delivery. The mesoporous n-HA was synthesized using the wet precipitation in the presence of cetyltrimethylammonium bromide (CTAB) at ambient temperature and normal atmospheric pressure. The morphology, size, crystalline phase, chemical composition and textural characteristics of the product were well characterized by X-ray Powder Diffraction (XRD), Fourier Transform Infrared Spectroscopy (FTIR), Scanning Electron Microscopy (SEM), Transmission Electron Microscopy (TEM), Dynamic Light Scattering (DLS) and N_2 adsorption/desorption, respectively. The protein adsorption/release studies were also carried out by using Bovine Serum Albumin (BSA) as a model protein. The results reveal that the mesoporous n-HA synthesized with CTAB exhibits high pure phase, low crystallinity and the typical characteristics of the mesostructure. The BSA loading increases with the specific surface area and the pore volume of n-HA, and the release rates of BSA are different due to their different pore sizes and pore structures. n-HA synthesized with 0.5% CTAB has the highest BSA loading and the slowest release rate because of its highest surface area and smaller pore size. These mesoporous n-HA materials demonstrate a potential application in the field of protein delivery due to their bioactive, biocompatible and mesoporous properties.

Keywords: hydroxyapatite, nanoparticles, mesostructure, cetyltrimethylammonium bromide, drug delivery

doi: 10.1016/S1672-6529(11)60105-4

1 Introduction

Hydroxyapatite ($Ca_{10}(PO_4)_6(OH)_2$, HA), the major inorganic constituent of natural bones and teeth, has been widely used for biomedical applications during the past decades due to its biocompatibility and bioactivity[1–3]. Synthetic nano-HA (n-HA) is one of attractive HA materials for bone regeneration owing to its similarity in composition to the mineral phase of native bone. It can be used as fillers of polymer composites to avoid the poor bioresorbability and brittle characteristics of HA ceramics or micro HA particles[3–5]. Meanwhile, the specific nano properties, such as small size, high surface area, low density, and high surface-to-volume ratio, open new domains of application for HA materials. It has been used as drug storage/release system to carry protein drugs for tissue engineering or other therapeutic purpose, such as growth factors[6,7].

Many fabrication techniques have been utilized to produce various HA nanomaterials, including sol–gel method[8], hydrothermal method[9], microemulsion process[10] and co-precipitation technique[11]. Among these methods, co-precipitation is the most common way for production of n-HA because of its simplicity and low cost and suitability for industrial production. However, the porous structure of n-HA is necessary for drug storage and release in many cases. Especially, mesoporous n-HA materials, those with pores of 2 nm–50 nm diameter, are becoming more imperative because they can be used as an novel effective drug storage/release system due to their large internal surface areas and narrow pore size distributions[12–14].

The surfactant-assisted method as one of the templating techniques, can produce HA nanomaterials with

Corresponding author: Jianguo Liu, Peibiao Zhang
E-mail: Jgliu2005@yahoo.com.cn, Zhangpb@ciac.jl.cn

mesopores[12,14]. The first nanostructured mesoporous material was reported by Beck *et al*. in 1992[15]. Although these materials can be fabricated directly with hydrothermal method[16] or co-precipitation technique[17], it is regarded that the most often-used method involves the use of surfactants as templates[12]. A series of surfactants, including pluronic P123[1,18], Sodium Dodecyl Sulfate (SDS)[19], and Cetyltrimethylammonium Bromide (CTAB)[20], have been used as templates for synthesis of mesoporous materials. The cooperative self-assembling of inorganic phases and surfactants produces a mesophase structure, and the removal of the organic component can produce well organized porous structures. Coelho *et al*.[20] synthesized HAp nanorods using CTAB and the effect of the sintering temperature on its nanostructure was studied. CTAB was chosen since it yields stable micelles, whose shape and size can be easily changed by modifying both the ratio and temperature of the solution.

In this paper, the mesoporous n-HA material was synthesized successfully using the wet precipitation in the presence of CTAB as a template. The objective of this work is to reveal the effect of surfactant ratio on the mesoporous n-HA, and the effect of the mesoporous structure on adsorption and release of BSA.

2 Materials and methods

2.1 Materials

Cetyltrimethylammonium bromide (CTAB) was purchased from Shanghai Huishi Chemical Co., Ltd.. Diammonium hydrogen phosphate ($(NH_4)_2HPO_4$), calcium nitrate tetrahydrate ($Ca(NO_3)_2{\cdot}4H_2O$) and ammonium hydroxide ($NH_3{\cdot}H_2O$) were purchased from Beijing Chemical Regent Co. Ltd.. Bovine Serum Albumin (BSA) (minimum 98%, electrophoresis grade) and BCA protein assay kit were purchased from Sigma-Aldrich. All other reagents and solvents were purchased from Sinopharm Chemical Reagent, China, and used as obtained. All chemicals were analytical grades and used directly without further purification.

2.2 Synthesis of mesoporous n-HA

The mesoporous n-HA particles were synthesized using the cationic surfactant method based on a modified method in the literature[20]. The chemical reaction equation is

$$10Ca(NO_3){\cdot}4H_2O+6(NH_4)_2PO_4+8NH_3{\cdot}H_2O \rightarrow Ca_{10}(PO_4)_6(OH)_2+20NH_4NO_3+6H_2O$$

A predetermined amount of surfactant CTAB, accounting for the theoretical yield of HA, 0.05%, 0.5%, 5% and 20% (w/w), were respectively dissolved in 50 ml of deionized water with overnight stirring at room temperature. $(NH_4)_2HPO_4$ (0.6 mol) was then added to the surfactant solution, and stirred well for 2 h. The CTAB/PO^{3-} solution was adjusted to pH 10.0 using $NH_3{\cdot}H_2O$. Separately, $Ca(NO_3)_2{\cdot}4H_2O$ (1 mol) was dissolved in 50 ml of water, and adjusted to pH 10.0 using $NH_3{\cdot}H_2O$. The Ca^{2+} solution was then slowly dropped into the CTAB/ PO^{3-} solution with continuous stirring and the solution was kept in pH 10.0 using $NH_3{\cdot}H_2O$. The reaction was undertaken with further stirring for 24 h at ambient temperature and normal atmospheric pressure. Finally, the mixture was centrifuged and washed repeatedly six times using deionized water and ethanol, and freeze-dried (−70 ˚C 48 hours) to obtain mesoporous n-HA. For comparison, parallel experiments were also carried out in the absence of CTAB. The obtained particles synthesized with different ratios of CTAB (0, 0.05%, 0.5%, 5% and 20%) were collected and coded as HA-0, HA-0.05, HA-0.5, HA-5 and HA-20, respectively. The particles were then ground in an agate mortar for further characterization.

2.3 Characterization

2.3.1 X-ray Diffraction

The phase and crystallographic structures of the synthesized n-HA were characterized by powder X-ray Diffraction (XRD) at room temperature. The analyses were undertaken using a Bruker D8 Advanced diffractometer with CuKa radiation of wavelength 1.541874Å, and a graphite monochromator running at 40 kV and 30 mA. The reconnaissance data were collected by loading the powder in glass holders and scanning from 10˚ to 80˚ in 0.02˚ steps of 2θ, with a dwell time of 2 s.

2.3.2 Fourier Transform Infrared Spectroscopy

The chemical and structural compositions of the samples were studied by a Bruker Vertex×70 Fourier Transform Infrared Spectroscopy (FTIR) in the frequency range 4000 cm^{-1}–400 cm^{-1}. The samples were mixed with KBr powders and pressed into a disk suitable for FTIR measurement. The functional groups presented in the particles were characterized and identified by their

peaks as obtained in the spectra.

2.3.3 Field Emission Scanning Electron Microscope

The particle morphology of the samples was observed using a Philips XL30 field Emission Scanning Electron Microscope (ESEM). Samples were first coated with platinum before microscopy and the images were collected at an accelerating voltage of 20 keV.

2.3.4 Transmission Electron Microscope

The Transmission Electron Microscopy (TEM) was used to observe the size and shape of n-HA samples. The powders of n-HA were ultrasonically dispersed in ethanol for 30 min and a drop of suspension was deposited on carbon-coated copper grids. Data were collected digitally using a FEI Tecnai G2 S-Twin TEM with an accelerating voltage of 200 kV.

2.3.5 Dynamic Light Scattering measurement

The particle size was measured by Dynamic Light Scattering (DLS) method using a Wyatt DAWN EOS Multi-angle Light Scattering (MALS) instrument equipped with a Wyatt QELS detector. The samples were well suspended in ethanol and diluted to 0.5 $mg \cdot ml^{-1}$. The DLS measurements were carried out at room temperature and were clarified with 0.22 μm filters immediately prior to analysis.

2.3.6 Nitrogen adsorption analysis

Nitrogen (N_2) adsorption-desorption isotherms were collected in a Quantachrome Autosorb-1 gas adsorption analyzer at 77 K after degassing the samples at 473 K for 24 h. The surface areas of sample powders were calculated according to the Barrett-Emmett-Teller (BET) equation. The relative pressure P/P_0 of the isotherm was studied between 0.01 and 1.0. The pore parameters were calculated from the adsorption branches of the isotherm from the Barrett-Joyner-Halanda model. The types of isotherms were evaluated according to their shape and type of hysteresis between the adsorption-desorption modes.

2.4 Protein loading and release

Bovine Serum Albumin (BSA, MW= 66.430 kDa, Sigma) was used as a model protein in this study according to the literature[21]. In order to estimate the adsorptive amount of protein on n-HA, 0.25g of n-HA particles were immersed in 40 ml of the protein solution (1 $mg \cdot ml^{-1}$, 24 h, 37 ˚C). The slurry was centrifuged and the amount of protein in the supernatant was measured by BCA protein assay (Wave length = 562 nm, MTP32, Corona) to calculate the adsorbed amount of protein on n-HA. All experiments were carried out in triplicates. The ratio of the albumin protein adsorbed was calculated by using the calibration curve obtained for pure albumin. The 20 mg of n-HA-protein particles were immersed in phosphate buffer solution (pH = 7.0, 10 ml). At time interval of 2 h, 2 ml solutions were drew from the above solution, then added 2 ml fresh PBS. The ratio of the albumin protein in the 2 ml solution was measured by BCA protein assay. According to the calibration curve, the BSA released amount was easily calculated.

2.5 Statistical analysis

All experiments were carried out in triplicates. Quantitative data are expressed as mean ± standard deviation. Wherever appropriate, comparisons of means were carried out using Origin 8.0 (OriginLab Corporation, U.S.A.), with $p < 0.05$ considered statistically significant.

3 Results and discussion

Fig. 1 shows the XRD patterns of n-HA particles synthesized with different ratios of CTAB. The characteristic peaks of all samples, including the peaks at 2θ = 26.12˚ and 32.30˚, correspond well to the HA reflections (JCPDS card No. 9-432)[22]. There are no differences in XRD patterns between samples synthesized without CTAB and those synthesized with different ratios of CTAB. According to the phase analysis, all the samples

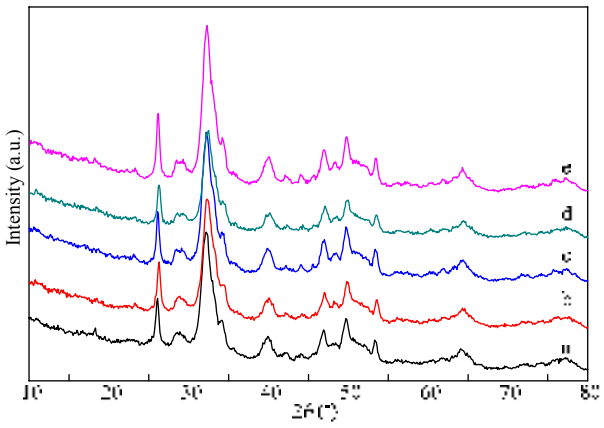

Fig. 1 XRD patterns of the n-HA particles: HA-0 (a), HA-0.05 (b), HA-0.5 (c), HA-5 (d) and HA-20 (e).

are phase-pure hydroxyapatite, and no characteristic peaks of impurities are observed in the patterns. Only minor differences are observed that the diffraction peaks of the samples synthesized are broader and less defined, showing low crystallinity. Furthermore, it is also revealed that standard hexagonal n-HA crystal has been formed. It is concluded that the existence of CTAB can not induce the crystallization of other phases and has little effect on the crystallization of n-HA.

Fig. 2 illustrates the FTIR spectra of the samples synthesized with different ratios of CTAB. The spectrum of HA-0 is identical to the representative spectrum of hydroxyapatite with phosphate stretching bands at about 900 cm^{-1} –1200 cm^{-1} and phosphate bending at 602 cm^{-1}[23]. But the characteristic absorption band of the hydroxyl group (3572 cm^{-1}) is almost absent in all the prepared samples due to the lower degree of crystallinity. According to the literature, the intensity of the hydroxyl band and the band at 961 cm^{-1} can be used as an indication of HA crystallinity[24]. The lower crystalline n-HA is easier to be absorbed than sintered n-HA or other calcium phosphates because of its higher dissolution rate[25]. The degradation of n-HA can lead to controllable, sustained delivery of the encapsulated drugs, which is an important factor for bone drug delivery systems. It is regarded that high crystalline HA may influence the drug release and inhibit real bone regeneration[26].

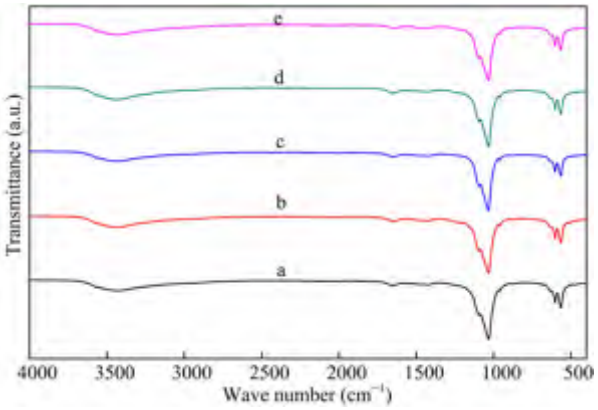

Fig. 2 FTIR spectra of the n-HA particles: HA-0 (a), HA-0.05 (b), HA-0.5 (c), HA-5 (d) and HA-20 (e).

Meanwhile, the FTIR spectra of n-HA synthesized with CTAB show all the characteristic bands of n-HA synthesized without CTAB. The broad bands around 3432 cm^{-1} and 1627 cm^{-1} are associated to the water molecules in the sample. The presence of the carbonate bands at 868 cm^{-1} and 1460 cm^{-1} in all the spectra is due to the presence of carbonate ions in the HA[27], which reveals that a certain level of carbonate substitution has taken place in the product. The carbonate ions may be originated from a reaction between atmospheric carbon dioxide and solution during the synthesis process. It has been shown that carbonate-containing HA has better bioactivity due to its similarity with human bone[28]. Therefore, the particles prepared in the study are expected to possess good biocompatibility.

Fig. 3 demonstrates the external morphology of the n-HA crystals prepared with different ratios of CTAB by the ESEM images. It is found that n-HA particles prepared with different ratios of CTAB (Figs. 3c–3j) are easier to assemble than those without CTAB (Figs. 3a and 3b). It is deduced that the different particle sizes and surface areas contribute to the distribution state of n-HA nanoparticles. Therefore, the size, the shape and the typical pore structure of the synthesized n-HA samples are further observed using TEM and DLS, as shown in Fig. 4. Both of n-HA nanoparticles synthesized with CTAB (Fig. 4a) and those without CTAB (Fig. 4b) are irregular crystals of about 10 nm × 45 nm, and the latter are longer and slender. It is verified by DLS analysis that the average size of HA-0 is 33.4 ± 13.2 nm in diameter, and those synthesized with CTAB are 12.8 nm–14.9 nm in diameter (Figs. 4c and 4d).

As shown in Fig. 5, the mesoporous structure of the n-HA nanoparticles is demonstrated by nitrogen adsorption analysis. Fig. 5 shows the respective N_2 adsorption/desorption isotherms of samples synthesized with different surfactant ratios. The particles prepared with CTAB (Figs. 5b–5e) exhibit the similar isotherms of type IV with the hysteresis loops of type H1, illustrating the properties of typical mesoporous materials with good pore accessibility[29]. Although HA-0 (Fig. 5 a) shows the similar isotherms, its larger limiting adsorption at high P/P_o indicates that there are a few quantity of smaller pores formed on the surface of these particles[16]. The results illustrate that the formation of mesoporous ma terials is guided by adding surfactants. CTAB is amphiphilic molecules, which has hydrophobic tail and hydrophilic head. They will form the micelles and act as the nucleation centre for the growth of n-HA crystals after they are completely dissolved and dispersed into monomers in aqueous solution[30]. The mesopores will be generated as soon as the surfactant is removed by washing.

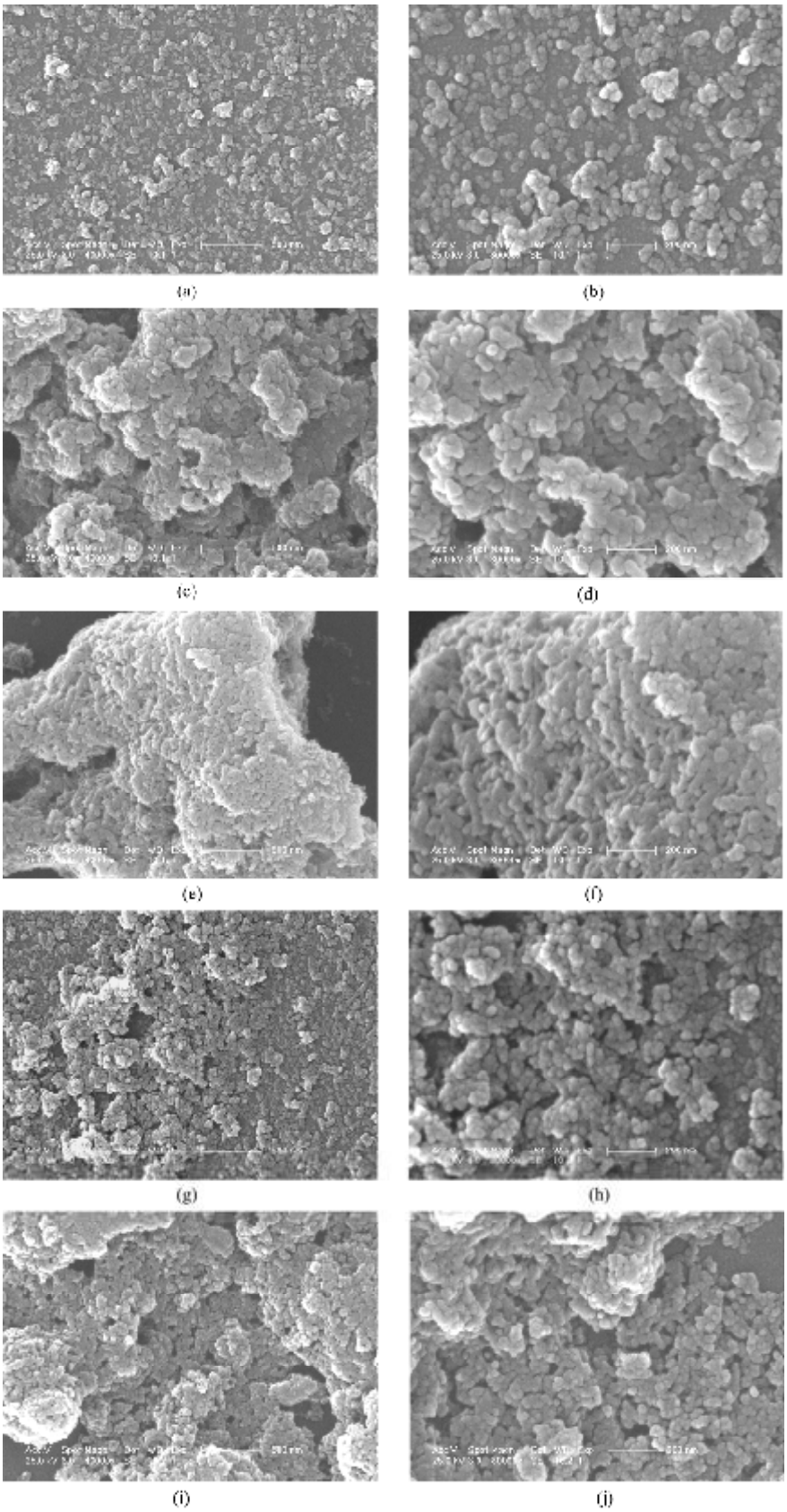

Fig. 3 SEM images of the n-HA particles: HA-0 (a and b), HA-0.05 (c and d), HA-0.5 (e and f), HA-5 (g and h) and HA-20 (i and j). Scale bars are 500 nm (a, c, e, g and i), and 200 nm (b, d, f, h and j).

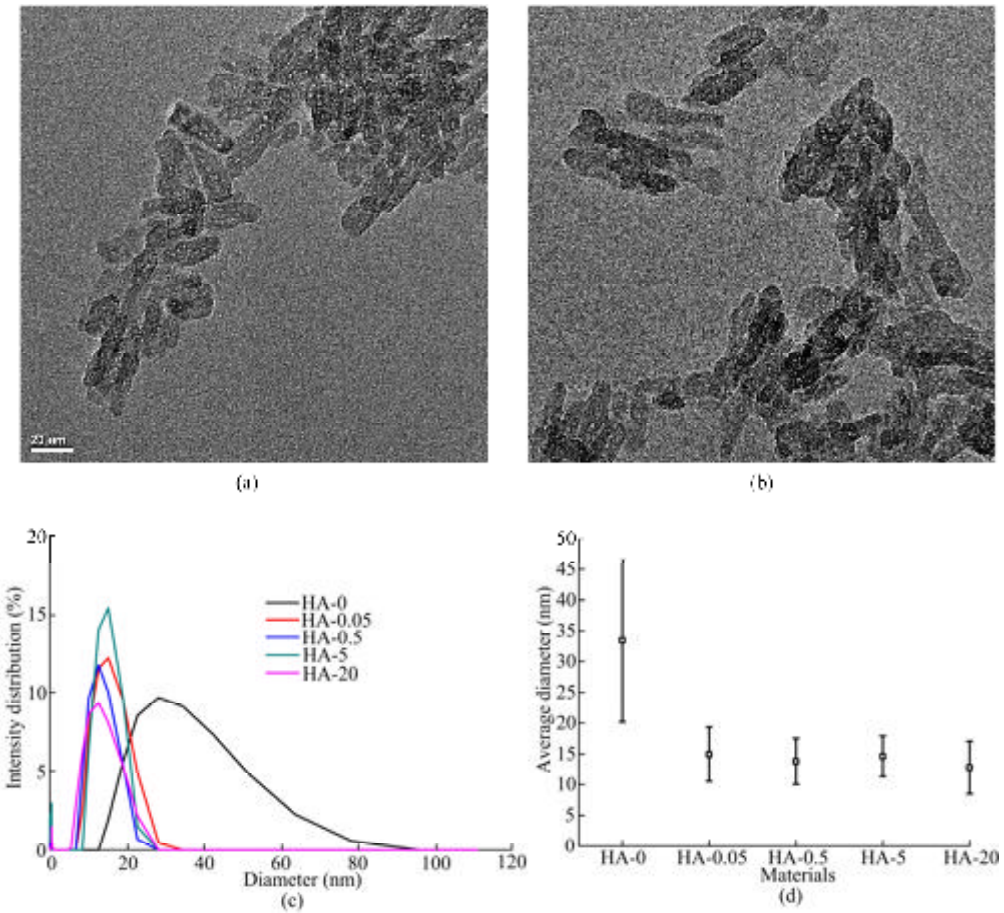

Fig. 4 TEM images of (a) HA-0 and (b) HA-0.5 particles. DLS analysis of (c) particle size distributions and (d) average diameters .

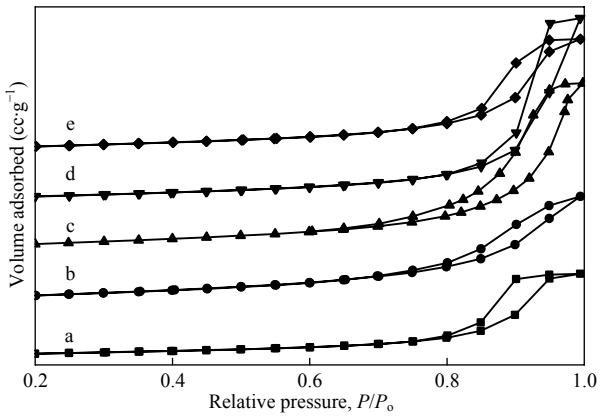

Fig. 5 N_2 adsorption/desorption isotherms of the n-HA particles: (a) HA-0,(b) HA-0.05, (c) HA-0.5, (d) HA-5 and (e) HA-20.

The textural parameters of the samples synthesized with different ratios of CTAB are summarized in Table 1. HA-0, which was prepared without surfactant, has BET surface area S_{BET} of 137.4 $m^2 \cdot g^{-1}$. However, the BET surface areas of the n-HA synthesized with CTAB are 179.8 $m^2 \cdot g^{-1}$–264.5 $m^2 \cdot g^{-1}$, greatly higher than that of HA-0. The differences in BET surface area might contribute to the smaller particle size and the larger pore volume of the mesoporous n-HA synthesized with CTAB. Moreover, the BET surface area of the particles increases with the ratio of surfactant from 0.05% to 0.5%, but decreases when the ratio of CTAB is further increased. When the ratio is 0.5%, the BET surface area is the largest (264.5 $m^2 \cdot g^{-1}$). The pore volume V_p is also shown in Table 1, illustrating the same trend as the BET surface area. However, the average pore size D_p shows the reverse trend among the n-HA particles synthesized with CTAB compared with the BET surface area and the

Table 1 The textural parameters of samples analyzed with nitrogen adsorption-desorption method

Samples	S_{BET} ($m^2 \cdot g^{-1}$)	V_p ($cm^3 \cdot g^{-1}$)	D_p (nm)
HA-0	137.4	0.17	4.9
HA-0.05	230.6	0.70	12.2
HA-0.5	264.5	0.95	11.3
HA-5	189.4	0.43	24.8
HA-20	179.8	0.30	29.1

pore volume although those of n-HA synthesized with CTAB are 11.3 nm–29.1 nm and also greatly higher than that of HA-0 (4.9 nm). The average pore size of HA-0.5 is 11.3 nm, which is smaller than those of other samples synthesized with CTAB. The pore size increases with the ratio of CTAB from 0.5% to 20%. Meanwhile, the pore size distribution of n-HA particles is analyzed as shown in Fig. 6. Compared with HA-0, the samples synthesized with different surfactant ratios exhibit a wider size distribution, and a small population with larger pore size may result from the particle aggregation as shown in above-mentioned SEM analysis. HA-0.05 and HA-0.5 have the similar size distributions which are greatly different from those of HA-5 and HA-20. The results indicate that the pore size is tightly associated with the ratio of surfactant. The mechanism is deduced that higher ratio of surfactant will result in more micelles or even morphology change of micelles and these micelles used as templates will further induce larger pore formation of n-HA particles. The similar results have been reported by Ng *et al.*[1] that the pore diameter of Mesostructured Calcium Phosphate (MCP) particles can be influenced by the concentration of surfactants (F127 and P123). Other researchers try to control the pore size of mesoporous materials with the chain lengths of templating molecules[31]. It is regarded that the loading efficiency and release rate of protein drugs are related to the surface area and the pore size of mesoporous materials[1].

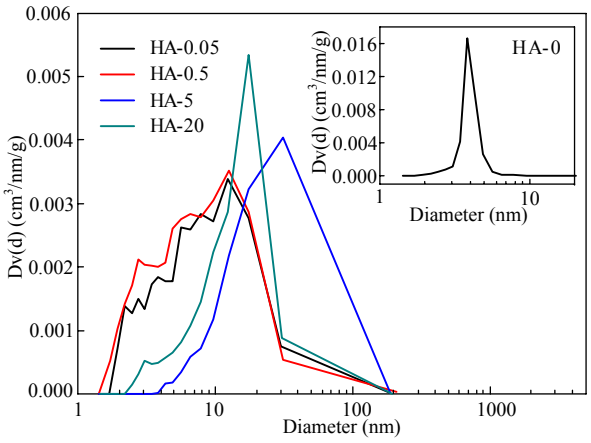

Fig. 6 The pore size distribution of mesoporous n-HA particles.

The loading efficiency of different n-HA samples with protein was studied with loading n-HA particles with BSA. Fig. 7 shows the cumulative loading amount of BSA in n-HA particles after 24 h immersion. The results show that the adsorbed amount of protein on n-HA has a high correlation with the specific surface area and pore volume of n-HA. All n-HA samples synthesized with CTAB have significantly superior protein loading properties compared with those without CTAB due to their higher BET surface area. Among the n-HA materials synthesized with CTAB, the sample of HA-0.5 shows the highest amount of adsorbed protein.

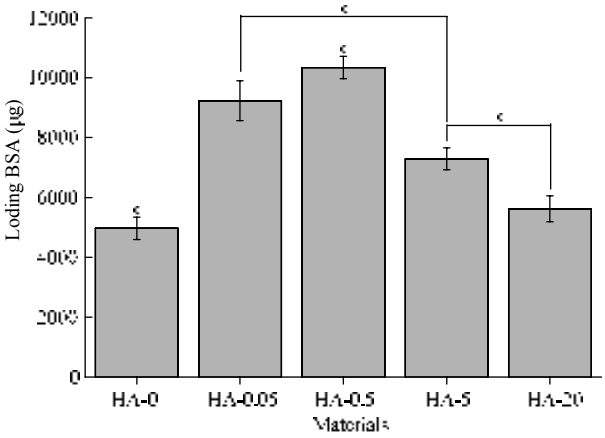

Fig. 7 The loading amount of BSA after 24 hours immersion.

The cumulative percentage of *in vitro* BSA release at various time intervals is shown in Fig. 8. All samples show an initial burst release of about 25%–47% BSA within the first 2 h, which may be attributed to the BSA weakly adsorbed on the outer surface of mesoporous hydroxyapatite. The 100% release is reached after 8 h and 10 h observed for HA-20 and HA-0, respectively. The main reason of the rapidest release observed in HA-20 and HA-0 is deduced that HA-20 has the largest pore size while HA-0 has the smallest pore volume and the smallest pores. According to the N_2 adsorption/desorption isotherms, the most pores of HA-0 are of micropores that are too small to allow the protein loading. However, the release is slower for HA-0.05, HA-0.5 and HA-5 after 2 h, and their release is then up to a stage after 16 h. The 24-hour release of HA-0.05, HA-0.5 and HA-5 is 80.1%, 75% and 98.6%, respectively. Among them, HA-0.5 has the lowest protein release rate due to its highest pore volume and smallest pore size. According to the release pattern, it is estimated that HA-0.05 and HA-0.5 will have the longest time to release. Thus the different release activities may mainly result from the pore size and the pore structure.

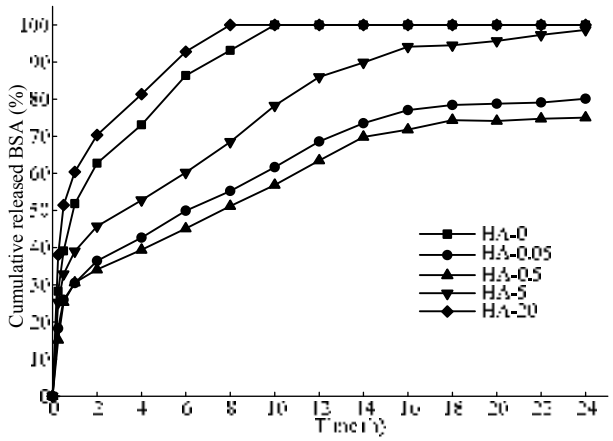

Fig. 8 BSA release rates of the samples in PBS for 24 hours.

HA materials have been widely used for protein drugs delivery because HA has two different binding sites, the C and the P sites on its surface respectively, which can provide proteins a multiple site binding opportunity[32]. The C sites are rich in calcium ions or positive charge and thus bind to acidic groups of proteins, but the P sites lack calcium ions or positive charge and therefore attach to basic groups of proteins[33]. On the other hand, the pore size of mesoporous n-HA is another key factor for suitable protein to penetrate into mesopores. The equivalent diameter of the BSA protein is 5.38 nm[34], which is less than the mesopore size of n-HA synthesized with CTAB in present study. It will provide the possibility for the proteins to reach and be adsorbed on the inner surface of mesopores. It is verified by the results of this study that the mesoporous n-HA synthesized with CTAB, especially synthesized with the ratio of 0.05%–5%, have superior protein loading properties compared with n-HA synthesized without CTAB. Specific recognition of proteins is a major ambition in the application of nanoparticles in the biological field. The specificity of nanoparticles-protein interactions is essential in a wide variety of processes including biodistribution, cell adhesion, inflammation and compatibility[35].

4 Conclusions

In present study, mesoporous nano-hydroxyapatite particles were successfully synthesized by low-temperature coprecipitation method in the presence of CTAB. The cationic surfactant of CTAB was used as a template to regulate n-HA crystal nucleation and growth. The results show that the synthesized particles have the features of high pure phase, low crystallinity and mesoporous structure. The ratio of surfactant effectively influences the mesoporous structure of n-HA particles, including the surface area, the pore volume and the pore size. The adsorbed amount of BSA on n-HA increases with the specific surface area and the pore volume, and the release rates of BSA are different due to the different pore sizes and pore structures. The n-HA particles synthesized with 0.5% CTAB exhibit the highest BSA loading and the slowest release rate due to its highest specific surface area and the smaller pore size, indicating that it has optimal mesoporous structure for good loading and well controlled release of BSA. These mesoporous n-HA materials demonstrate a potential application in the field of protein delivery due to their bioactive, biocompatible and mesoporous properties.

Acknowledgments

We gratefully acknowledge the financial support from the National Natural Science Foundation of China (No.50733003 and No.50973109), the Major Project of International Cooperation from the Ministry of Science and Technology of China (2010DFB50890) and the Interdiscipline Subject Project from Jilin University (2011J018).

References

[1] Ng S X, Guo J, Ma J, Loo S C J. Synthesis of high surface area mesostructured calcium phosphate particles. *Acta Biomaterialia*, 2010, **6**, 3772–3781.

[2] Zhang Y F, Cheng X R, Chen Y, Shi B, Chen X H, Xu D X, Ke J. Three-dimensional nanohydroxyapatite/chitosan scaffolds as potential tissue engineered periodontal tissue. *Journal of Biomaterials Applications*, 2007, **21**, 333–349.

[3] Zeng S, Fu S Z, Guo G, Liang H, Qian Z Y, Tang X H, Luo F. Preparation and characterization of nano-hydroxyapatite/poly(vinyl alcohol) composite membranes for guided bone regeneration. *Journal of Biomedical Nanotechnology*, 2011, **7**, 549–557.

[4] Zhang P B, Hong Z K, Yu T, Chen X S, Jing X B. In vivo mineralization and osteogenesis of nanocomposite scaffold of poly (lactide-co-glycolide) and hydroxyapatite surface-grafted with poly(L-lactide). *Biomaterials*, 2009, **30**, 58–70.

[5] Paul W, Sharma C P. Development of porous spherical hydroxyapatite granules: Application towards protein

delivery. *Journal of Materials Science*: *Materials Medicine*, 1999, **10**, 383–388.

[6] Itoh S, Kikuchi M, Koyama Y, Matumoto H N, Takakuda K, Shinomiya K, Tanaka J. Development of a novel biomaterial, hydroxyapatite/collagen (HAp/Col) composite for medical use. *Bio-Medical Materials and Engineeing*, 2005, **15**, 29–41.

[7] Liu T Y, Chen S Y, Liu D M, Liou S C. On the study of BSA-loaded calcium-deficient hydroxyapatite nano-carriers for controlled drug delivery. *Journal of Controlled Release*, 2005, **107**, 112–121.

[8] Padmanabhan S K, Balakrishnan A, Chu M C, Lee Y J, Kim T N, Cho S J. Sol–gel synthesis and characterization of hydroxyapatite nanorods. *Particuology*, 2009, **7**, 466–470.

[9] Zhang C, Li C, Huang S, Hou Z, Cheng Z, Yang P, Peng C, Lin J. Self-activated luminescent and mesoporous strontium hydroxyapatite nanorods for drug delivery. *Biomaterials*, 2010, **31**, 3374–3383.

[10] Bose S, Saha S K. Synthesis and characterization of hydroxyapatite nanopowders by emulsion technique. *Chemistry of Materials*, 2003, **15**, 4464–4469.

[11] Wu H C, Wang T W, Sun J S, Wang W H, Lin F H. A novel biomagnetic nanoparticle based on hydroxyapatite. *Nanotechnology*, 2007, **18**, 165601.

[12] Ying J Y, Mehnert C P, Wong M S. Synthesis and applications of supramolecular-templated mesoporous materials. *Angewandte Chemie International Edition*, 1999, **38**, 56–77.

[13] Jiang J H, Fan Y, Zhang L R, Yang H, Chen Y L, Zhao D Z, Zhang P. Synthesis and characterization of multi-lamellar mesostructured hydroxyapatites using a series of fatty acids. *Journal of Materials Science*, 2011, **46**, 3828–3834.

[14] Li Y, Tjandra W, Tam K C. Synthesis and characterization of nanoporous hydroxyapatite using cationic surfactants as templates. *Materials Research Bulletin*, 2008, **43**, 2318–2326.

[15] Beck J S, Vartuli J C, Roth W J, Leonowicz M E, Kresge C T, Schmitt K D, Chu C T W, Olson D H, Sheppard E W. A new family of mesoporous molecular sieves prepared with liquid crystal templates. *Journal of the American Chemical Society*, 1992, **114**, 10834–10843.

[16] Guo Y P, Yao Y B, Ning C Q, Guo Y J, Chu L F. Fabrication of mesoporous carbonated hydroxyapatite microspheres by hydrothermal method. *Materials Letters*, 2011, **65**, 2205–2208.

[17] Parida K, Naik B. Synthesis of mesoporous TiO2á-áxNx spheres by template free homogeneous co-precipitation method and their photo-catalytic activity under visible light illumination. *Journal of Colloid and Interface Science*, 2009, **333**, 269–276.

[18] Li Y B, Li D X, Xu Z Z. Synthesis of hydroxyapatite nanorods assisted by Pluronics. *Journal of Materials Science*, 2009, **44**, 1258–1263.

[19] Zhang J, Fujiwara M, Xu Q, Zhu Y, Iwasa M, Jiang D. Synthesis of mesoporous calcium phosphate using hybrid templates. *Microporous and Mesoporous Materials*, 2008, **111**, 411–416.

[20] Coelho J M, Moreira J A, Almeida A, Monteiro F J. Synthesis and characterization of HAp nanorods from a cationic surfactant template method. *Journal of Materials Science: Materials in Medicine*, 2010, **21**, 2543–2549.

[21] Xia W, Chang J. Well-ordered mesoporous bioactive glasses (MBG): A promising bioactive drug delivery system. *Journal of Controlled Releas*e, 2006, **110**, 522–530.

[22] Ramachandran R, Paul W, Sharma C P. Synthesis and characterization of PEGylated calcium phosphate nanoparticles for oral insulin delivery. *Journal of Biomedical Materials Research Part B*, 2009, **88**B, 41–48.

[23] Chandra Sharma P, Chandy T. Influence of steroid hormones on protein-platelet interaction at the blood-polymer interface. *Biomaterials*, 1989, **10**, 609–616.

[24] Liu J B, Li K W, Wang H, Zhu M K, Xu H Y, Yan H. Self-assembly of hydroxyapatite nanostructures by microwave irradiation. *Nanotechnology*, 2005, **16**, 82.

[25] Oonishi H, Hench L L, Wilson J, Sugihara F, Tsuji E, Kushitani S, Iwaki H. Comparative bone growth behavior in granules of bioceramic materials of various sizes. *Journal of Biomedical Materials Research*, 1999, **44**, 31–43.

[26] Matsumoto T, Okazaki M, Inoue M, Yamaguchi S, Kusunose T, Toyonaga T, Hamada Y. Hydroxyapatite particles as a controlled release carrier of protein. *Biomaterials*, 2004, **25**, 3807–3812.

[27] Holcomb D, Young R. Thermal decomposition of human tooth enamel. *Calcified Tissue International*, 1980, **31**, 189–201.

[28] Panda R, Hsieh M, Chung R, Chin T. FTIR, XRD, SEM and solid state NMR investigations of carbonate-containing hydroxyapatite nano-particles synthesized by hydroxide-gel technique. *Journal of Physics and Chemistry of Solids*, 2003, **64**, 193–199.

[29] Sing K S W, Everett D H, Haul R A W, Moscou L, Pierotti R A, Rouquerol J, Siemienewska T. Reporting physisorption data for gas/solid systems with special reference to the determination of surface area and porosity (recommendations 1984). *Pure and Applied Chemistry*, 1985, **57**, 603–619.

[30] Shanthi P, Mangalaraja R, Uthirakumar A, Velmathi S, Balasubramanian T, Ashok M. Synthesis and characteriza-

tion of porous shell-like nano hydroxyapatite using cetrimide as template. *Journal of Colloid and Interface Science*, 2010, **350**, 39–43.

[31] Wong M S, Ying J Y. Amphiphilic templating of mesostructured zirconium oxide. *Chemistry of Materials*, 1998, **10**, 2067–2077.

[32] Kawasaki T, Takahashi S, Ideda K. Hydroxyapatite high-performance liquid chromatography: Column performance for proteins. *European Journal of Biochemistry*, 1985, **152**, 361–371.

[33] Kandori K, Masunari A, Ishikawa T. Study on adsorption mechanism of proteins onto synthetic calcium hydroxyapatites through ionic concentration measurements. *Calcified Tissue International*, 2005, **76**, 194–206.

[34] Fuss C, Palmaz J C, Sprague E A. Fibrinogen: Structure, function, and surface interactions. *Journal of Vascular and Interventional Radiology*, 2001, **12**, 677–682.

[35] Aggarwal P, Hall J B, McLeland C B, Dobrovolskaia M A, McNeil S E. Nanoparticle interaction with plasma proteins as it relates to particle biodistribution, biocompatibility and therapeutic efficacy. *Advanced Drug Delivery Reviews*, 2009, **61**, 428–437.